Meteoritics & Planetary Science 39, Nr 2, 303–320 (2004)
Abstract available online at http://meteoritics.org

Experimental ejection angles for oblique impacts: Implications for the subsurface flow-field

Jennifer L. B. ANDERSON,[1*] Peter H. SCHULTZ,[1] and James T. HEINECK[2]

[1]Geological Sciences, Brown University, Providence, Rhode Island 02912, USA
[2]Experimental Physics Group, NASA Ames Research Center, Moffett Field, California 94035, USA
[*]Corresponding author. E-mail: Jennifer_Anderson@brown.edu

(Received 11 July 2003; revision accepted 5 September 2003)

Abstract–A simple analytical solution for subsurface particle motions during impact cratering is useful for tracking the evolution of the transient crater shape at late times. A specific example of such an analytical solution is Maxwell's Z-Model, which is based on a point-source assumption. Here, the parameters for this model are constrained using measured ejection angles from both vertical and oblique experimental impacts at the NASA Ames Vertical Gun Range. Data from experiments reveal that impacts at angles as high as 45° to the target's surface generate subsurface flow-fields that are significantly different from those created by vertical impacts. The initial momentum of the projectile induces a subsurface momentum-driven flow-field that evolves in three dimensions of space and in time to an excavation flow-field during both vertical and oblique impacts. A single, stationary point-source model (specifically Maxwell's Z-Model), however, is found inadequate to explain this detailed evolution of the subsurface flow-field during oblique impacts. Because 45° is the most likely impact angle on planetary surfaces, a new analytical model based on a migrating point-source could prove quite useful. Such a model must address the effects of the subsurface flow-field evolution on crater excavation, ejecta deposition, and transient crater morphometry.

INTRODUCTION

Point-source theory assumes that, during an impact, the portion of the target material affected by the initial conditions (projectile mass, velocity, density, and impact angle) is small. Therefore, the impact can be treated as a simple point-source at distances that are large compared to the projectile diameter and on time scales that are large compared to the time needed to deposit the projectile's momentum and energy into the target (Holsapple and Schmidt 1987). Two main lines of evidence support the assumption that such a point-source model is appropriate for use in impact cratering: the general similarity of explosion and impact craters for the appropriate equivalent depth of burst and the resultant power-law forms of impact scaling relationships. One specific point-source approach is Maxwell's Z-Model (Maxwell 1973, 1977; Orphal 1977). This analytic and quantitative model predicts a number of features of the impact process: the subsurface flow-field, crater shape and volume, and excavation parameters such as ejection speed and angle. No other point-source model has been developed to this degree of usefulness in describing the evolving flow-field.

The point-source approximation is based on experimental and computational data for near-surface explosions (e.g., Oberbeck 1971; Roddy 1976; Piekutowski 1977, 1980; Schmidt and Holsapple 1980) and vertical impacts (e.g., Oberbeck 1971; Stöffler et al. 1975; Gault and Wedekind 1977). Various aspects of vertical impacts (such as ejecta curtain shape, crater shape and volume, and subsurface deformation) can be matched reasonably well by the optimum burial of an explosive source (e.g., Oberbeck 1971; Cooper 1977; Oberbeck 1977; Holsapple 1980). Since experimental data for vertical impacts (such as scaled ejection speeds and crater volumes) fall along well-defined power-law relationships (e.g., Holsapple and Schmidt 1982; Housen et al. 1983; Schmidt and Housen 1987), a point-source is also implied (Holsapple 1993).

The question addressed in the present contribution is the extent to which a point-source approximation can replicate experimental observations of the excavation and growth of oblique impacts. Ejection angles are measured during oblique and vertical impacts at the NASA Ames Vertical Gun Range using three-dimensional particle image velocimetry (3D PIV) (Heineck et al. 2002; Anderson et al. 2003). Data are taken during the "first half of crater growth," defined here as the time it takes the transient crater radius to grow to half the final crater radius. These experiments address the excavation stage of crater growth when target material is leaving the surface along independent ballistic trajectories. The measured ejection angles are used to constrain the point-source parameters of Maxwell's Z-Model. Such a strategy tests the applicability of the Z-Model as a means of inferring the subsurface flow during vertical and oblique impacts.

Maxwell's Z-Model is only one specific example of a point-source model and is the most extensively used because of its simplicity and predictive nature. It is not derived from first principles; rather, it is empirical and analytical, based on observations and calculations of explosion cratering (Maxwell 1973). Such models are extremely useful because of their inherent analytical nature and ease in application. Numerical models from first-principles are typically constrained to the initial stages of impact cratering due to the amount of computer time and resources available. Two-dimensional simulations lend insight into the processes for vertical impacts by the assumption of cylindrical symmetry (Pierazzo and Melosh 2000b), while three 3-dimensional simulations are only beginning to assess the earliest processes in the excavation stage for oblique impacts (Pierazzo and Melosh 1999, 2000a; Artemieva and Pierazzo 2003). Furthermore, the later stages of cratering are dominated by material strength effects, which increase the complexity of the numerical models. Designing computer models that begin at the moment of impact and follow material motions through the end of the excavation stage requires significant effort and resources, even in two dimensions. Since oblique impacts are far more common than vertical impacts (Gilbert 1892; Shoemaker 1962), it would be useful to have a simple method of addressing the effect of obliquity on subsurface flow, excavation, ejecta deposition, and crater morphometry.

The following discussion first reviews the use of point-source models for impact cratering. Second, alterations to the Z-Model are described as it has been modified over time to replicate vertical impacts more accurately. Third, the method of measuring ejection angles in the laboratory using three-dimensional particle image velocimetry (3D PIV) is discussed. Data acquired using 3D PIV establish Z-Model parameters such as the depth of the flow-field center and the value of Z. While such modifications to the Z-Model are able to predict the general character of the subsurface flow-field, the same modifications are not yet accurate enough to predict finer details of impact cratering such as the range of ejection angles observed in experiments. Fourth, the limitations of the modified Z-Model for vertical and oblique impacts are discussed along with implications of this work for understanding their subsurface flow-fields. Last, further alterations to Maxwell's Z-Model and suggestions for a new analytical impact-cratering model are proposed to track the evolving flow-field created by an oblique impact.

BACKGROUND

Impacts as Point Sources

Point-source theory for impact cratering evolved from both experimental and numerical studies of explosion cratering. A point-source model is often used to approximate the effects of momentum and energy deposition from projectile to target material during an impact (e.g., Holsapple and Schmidt 1987), similar to the deposition from a chemical or nuclear source to the target during an explosion. It is possible to produce explosion craters that generally resemble impact craters in shape and morphology from laboratory to planetary scales (i.e., Roddy 1968; Oberbeck 1971; Roddy 1976; Schmidt and Holsapple 1980). Since planetary-scale impact craters are impossible to create experimentally, large-scale chemical and nuclear explosion craters provide a useful reference for understanding planetary impact craters.

Both impact and explosion craters deposit a large amount of energy into the near-surface target material in a very short amount of time (Baldwin 1963; Kreyenhagen and Schuster 1977). Consequently, both exhibit generally similar excavation over most of crater growth. Explosion cratering, however, cannot address a number of factors that are fundamental to the impact cratering process, such as the momentum of the projectile (e.g., Dienes and Walsh 1970) and the effects of projectile impact angle. For these reasons, explosion cratering is inherently an axially symmetric process, whereas impact cratering can be a very asymmetric process, even at relatively high impact angles (e.g., Schultz and Anderson 1996; Dahl and Schultz 2001; Anderson et al. 2003). Gases released from the chemical and nuclear reactions and the presence of an atmosphere during the formation of large-scale explosion craters in the field also modify the resultant ejecta dynamics.

Despite these important differences between the two processes, explosion-cratering studies have led to a number of concepts that have proved useful in understanding impact cratering. For example, explosion-cratering studies were used to develop the first scaling relationships for planetary-scale impact craters (Baldwin 1963; Chabai 1965, 1977). Point-source theory also predicts that scaling relationships for impact cratering should follow a power-law form (Holsapple 1993); indeed, many do throughout much of crater growth. Comparisons of small-scale impacts and explosions further revealed that explosions most closely replicate impacts when the explosive source is buried at a specific depth below the target surface, usually equivalent to 1–2 projectile radii (Oberbeck 1971, 1977). The necessity of including a term for the depth to the flow-field center during impacts illustrates the effect of the momentum deposition characterizing impacts and not explosions.

Dienes and Walsh (1970) first proposed that the relatively successful match between impacts and explosions resulted from a "late-stage equivalence" where details of the initial conditions of the impact or explosion were not important to the resultant material flow at distances relatively large compared to the source region. Holsapple and Schmidt (1987) further refined this approach by defining a "coupling parameter" that links the initial properties of the projectile to the intermediate and late-stage excavation flow. This coupling parameter is a combination of the projectile mass, velocity, and density that governs the excavation flow and can be applied in scaling relationships to derive final crater parameters. Comparisons between numerical and experimental explosions led to the development of analytical and empirical models, such as the Z-Model, for describing the general characteristics of the subsurface flow during explosion cratering and its implications for impact cratering.

Recent experimental studies demonstrate that shock asymmetries during oblique impacts persist well into the far field (Dahl and Schultz 2001) and ejecta excavation during oblique impacts is asymmetric, again persisting to relatively late times (Schultz and Anderson 1996; Anderson et al. 2003), well after the point-source flow-field would have been established for a vertical impact. While oblique impacts (even down to angles as low as 20°) can still produce circular craters in particulate targets (Gault and Wedekind 1978), the validity of applying point-source models to oblique impacts needs further testing. Consequently, the goal of this work is to assess one particular point-source model, the Z-Model, for predicting the excavation of both vertical and oblique experimental impacts.

Maxwell's Z-Model

Maxwell's Z-Model was determined empirically and analytically to describe the flow field associated with surface and near-surface chemical explosion craters (Maxwell 1973, 1977; Orphal 1977). By comparing a number of numerical calculations of near-surface explosion craters, Maxwell generalized the subsurface flow-field. The Z-Model is based on three main assumptions (Maxwell 1977): 1) subsurface material flow is incompressible; 2) material moves along independent, ballistic trajectories after detaching from the target near the surface plane; and 3) the subsurface radial component of velocity is given by:

$$u_R = \frac{\alpha(t)}{R^Z} \tag{1}$$

where R represents the radial distance from the flow-field center to the subsurface particle position, and u_R is the radial velocity of that particle. In general, α is a function of time and represents the strength of the flow along different streamlines. The value of Z characterizes the shape of the flow field and can vary from one streamline to another (distinguished by their initial location in Θ). The values of α and Z, however, are usually assumed to be constant. Although this does not conserve total energy in the flow, the assumption of constant α and Z agrees fairly well with numerical calculations of explosion craters (Maxwell 1973; Orphal 1977). The geometry for the Z-Model assumes axial symmetry (Fig. 1a). Note that the position of the flow-field center is the explosive source at the target surface. For impacts, the Z-Model assumes the flow-field center to be at the impact point, again at the target surface.

The subsurface streamlines defined by the Z-Model are logarithmic spirals that originate at the flow-field center and end at the target surface. Particles are then assumed to follow independent ballistic trajectories defined by the speed and angle of the particle as it passes through the plane of the target surface. Maxwell (1973) defined the streamline functions in polar coordinates (R, Θ) as:

$$R(t)^{Z+1} - R_o^{Z+1} = (Z+1)\alpha t \tag{2a}$$

$$\frac{1-\cos\Theta(t)}{1-\cos\Theta_o} = \left(\frac{R(t)}{R_o}\right)^{Z-2} \tag{2b}$$

where, at time t = 0, the particle's position is $R = R_o$ and $\Theta = \Theta_o$ (see Fig. 1a).

The value of Z characterizes the shape of the cratering flow-field and determines the curvature of the streamlines. By increasing Z, the streamlines curve more sharply and yield higher ejection angles at the target surface (Fig. 1b). Thus, radial flow in every direction away from the explosive source is defined by Z = 2. By conserving total vertical momentum and neglecting gravity, Maxwell (1977) found that $Z \approx 2.7$ is most appropriate for an explosion crater. The value of Z actually depends on the initial orientation of the streamline below the target surface (Θ_o) (Maxwell 1977). Therefore, directly below the impact point ($\Theta_o = 0°$), Z = 2 and material flows radially downward. Near the target surface ($\Theta_o = 90°$), material follows sharply curved streamlines upward and Z = 4.

Assuming constant α, constant Z, and an explosive charge at the target surface, Maxwell (1977) derived the ejection velocity of particles at the surface. The horizontal and vertical components of the ejection velocity are given respectively by:

$$u_H = \frac{\alpha}{r_o^Z} \tag{3a}$$

$$u_V = (Z-2)u_H \tag{3b}$$

where r_o is the ejection range or distance between the flow-field center and the ejection position. The ejection angle (θ_e) is easily calculated from Equation 3b:

$$\tan(\theta_e) = Z - 2 \tag{4}$$

where θ_e is measured from the surface of the target. The Z-Model, therefore, predicts a constant ejection angle independent of ejection position throughout crater growth, with the assumption that Z and α are constant in time and

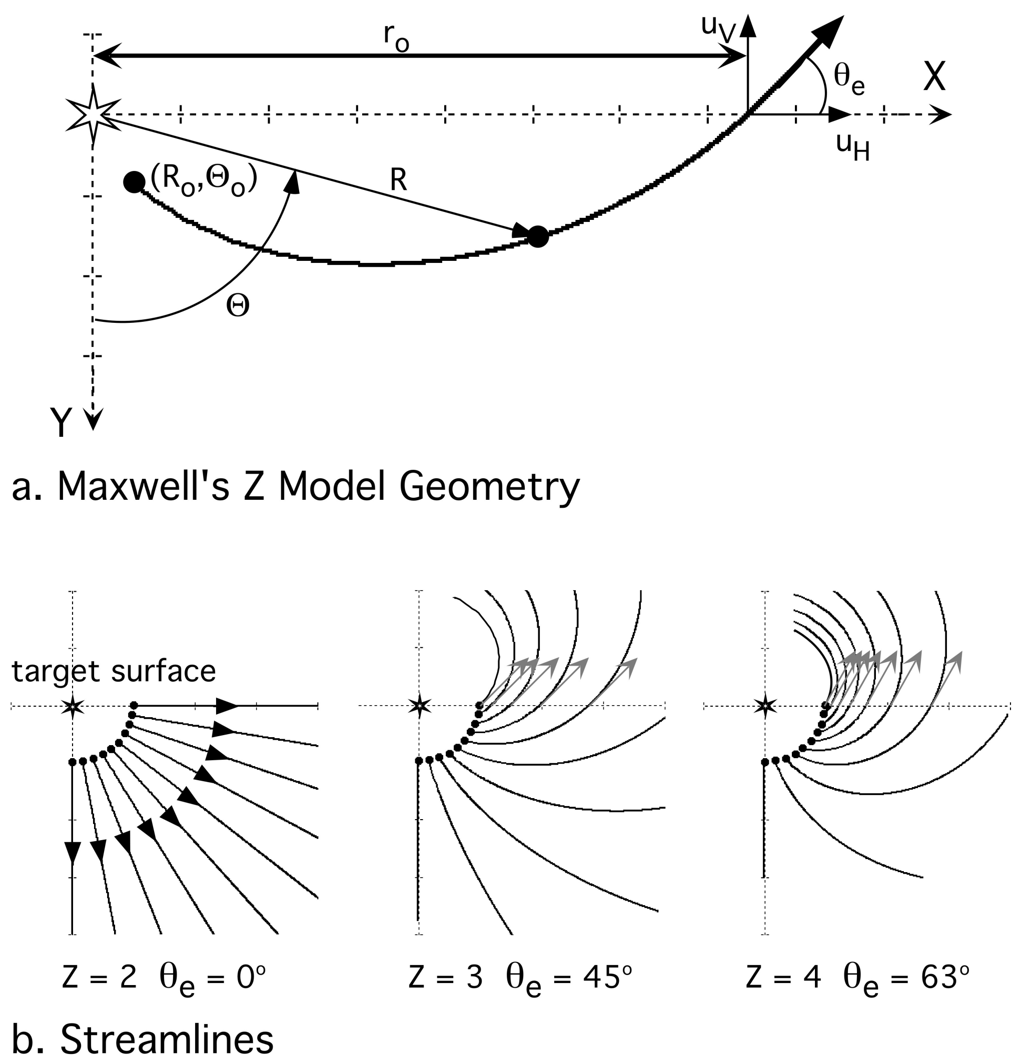

Fig. 1. a) The geometry of Maxwell's Z-Model, where the x-axis represents the target surface, and the star represents the explosive source; b) subsurface streamlines as predicted by the Z-Model. Note that the shape of the flow field changes for different values of Z. Each value of Z implies a different ejection angle, which remains constant throughout that crater's growth.

position. This ejection angle is completely determined by the value of Z (Fig. 1b).

The Z-model was widely used as a simple tool for approximating the complex material flow beneath the target surface during explosions and vertical impacts. A particular series of studies (Thomsen et al. 1979; Austin et al. 1980; Austin et al. 1981) performed detailed numerical calculations of both laboratory- and planetary-scale vertical impacts and compared the resulting flow-fields to those predicted by the Z-Model. These studies concluded that the Z-Model was a useable tool overall for modeling the subsurface flow of material during the excavation stage for impacts provided that two main modifications were made. First, the values of both Z and α varied with time throughout the compression stage and into the excavation stage (where the numerical code ended). Second, the flow-field center, which is assumed to be located at the explosive source, needed to be buried beneath the target surface by one projectile radius. This depth to the flow-field center, however, also changed with time and was found to migrate downward along the impact axis as the crater grew. The need for incorporating the depth of the flow-field center into the Z-Model when applied to impact cratering explicitly captured the effect of the initial momentum of the projectile on the subsurface cratering flow-field, which is absent in explosion craters.

The Modified Z-Model

Croft (1980) modified the Z-Model to incorporate a depth to the flow-field center (Fig. 2). In general, Croft simply moved Maxwell's streamlines below the target surface by a constant amount that represented the depth to the flow-field center. Now, instead of the explosive source being located at the target surface, it is buried a certain depth, d. The

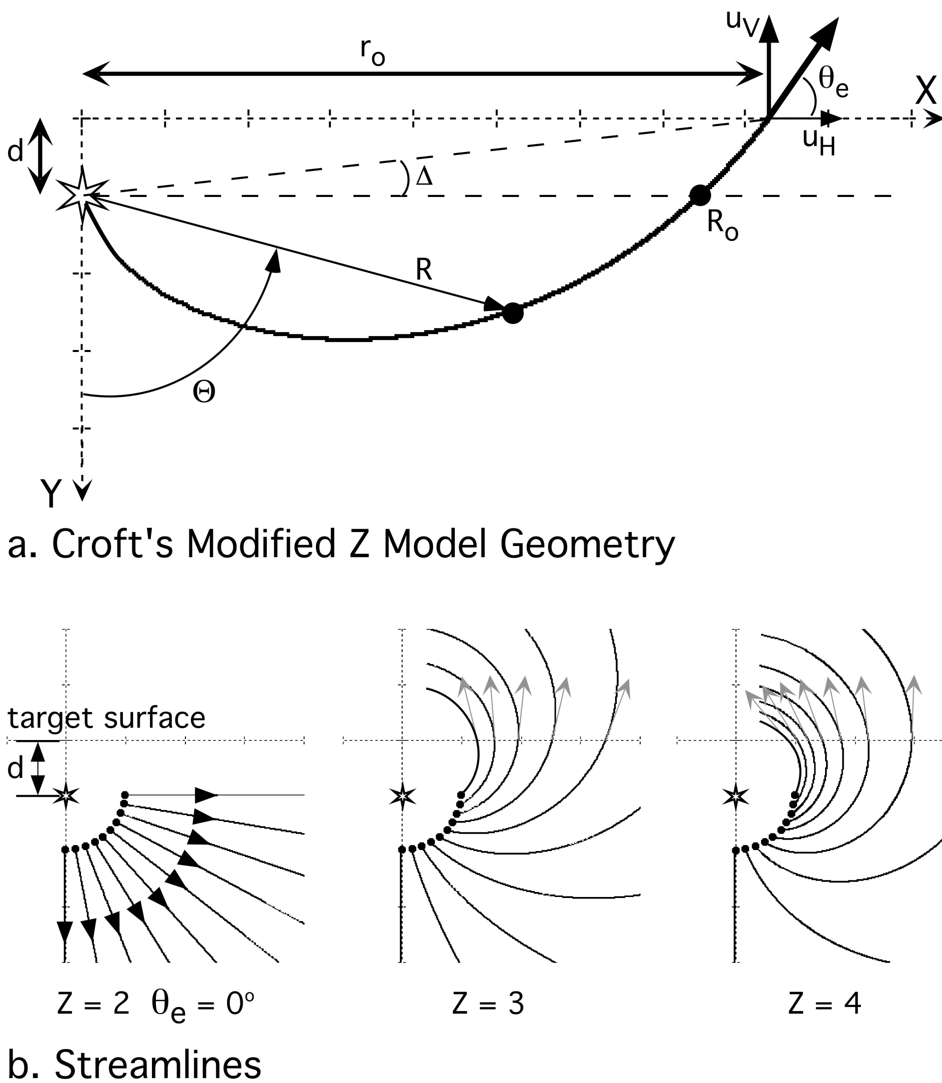

Fig. 2. Croft's modification to Maxwell's Z-Model (a) geometry and (b) predicted subsurface streamlines. Compared to Fig. 1, the streamlines are simply shifted beneath the target surface (represented by the x-axis) by a constant amount, d. This allows ejection angles to decrease as the crater grows. For Z = 2, the flow is radial away from the explosive source (represented by the star). When Z >2, material is ejected at angles initially higher than 90° that then decrease as the crater grows.

origin of Croft's polar coordinate system is located at the explosive source, a depth, d, below the target surface. The streamline equation in polar coordinates is given as:

$$R = R_o(1-\cos\Theta)^{\frac{1}{Z-2}} \tag{5a}$$

where R_o is a reference radius at which the streamline passes through the horizontal plane located at the depth to the flow-field center, d (Θ_o = 90°). The origin of Croft's rectangular coordinate system is located at the target surface, yielding the following streamline equations:

$$X = R_o \sin\Theta \tag{5b}$$

$$Y = R_o\cos\Theta(1-\cos\Theta)^{\frac{1}{Z-2}} + d \tag{5c}$$

The predicted ejection angles then become:

$$\tan\theta_e = \frac{\frac{\tan\Delta}{\cos\Delta} - \tan^2\Delta + (Z-2)}{\frac{1}{\cos\Delta} - \tan\Delta(Z-1)} \tag{6a}$$

where

$$\tan\Delta = \frac{d}{r_o} \tag{6b}$$

or the ratio of the depth to the flow-field center, d, and the horizontal distance along the target surface between the ejection position and the flow-field center, r_o (geometry shown in Fig. 2a). When the flow-field center is located at the target surface (d = 0 and Δ = 0°), Equation 6 reduces to

Maxwell's predicted ejection angle (Equation 4). Croft's "Modified Z-Model," as represented by Equations 5 and 6, will hereafter be referred to as the MZ-Model.

Maxwell developed the Z-Model as a simple means to describe particle velocities in flow fields generated by explosion-cratering calculations. In the absence of any other equivalent analytical model, the Z-Model and Croft's modification of the Z-Model have been used to approximate many features of impact cratering that are difficult to observe in the laboratory or achieve through numerical modeling. The Z-Model has been used to estimate excavation volumes for terrestrial craters (e.g., Grieve and Cintala 1981), subsurface material displacements (e.g., Turtle et al. 2003), and transient cavity shapes for the initial conditions needed for numerical investigations of the modification stage of cratering (e.g., Collins et al. 2002). This study will compare Z-Model predictions to observed excavation data during vertical and oblique experimental impacts. Although the Z-Model and the MZ-Model both assume axial symmetry and, thus, are unable to model directly the three-dimensional nature of oblique impacts, it is, nonetheless, of interest to see how well the models do, the nature of the deficiencies, and what such comparisons can suggest regarding the nature of the flow field for oblique impacts—the essence of this study.

EXPERIMENTAL DESIGN

The experiments used in the present study were performed at the NASA Ames Vertical Gun Range (AVGR), a national impact-cratering facility capable of impact angles from 15° to 90° from horizontal (see description in Gault and Wedekind [1978]). All the experiments described below were low-velocity (near 1 km/s) impacts of 6.35 mm aluminum spheres into a medium-grained (0.5 mm) particulate sand target under a vacuum of less than 7×10^{-4} atm. The impact angle varied from vertical (90°) to 60°, 45°, 30°, and 15° above horizontal. Low velocities were used to provide benchmarks for higher velocity experiments (to be discussed in a separate paper). Additionally, the ratio of momentum to energy is maximized for lower velocity impacts (e.g., Schultz 1988).

Three-dimensional particle image velocimetry (3D PIV) records individual ejecta particles in flight during crater excavation and measures ejecta particle velocities in three dimensions. A detailed description of the 3D PIV technique and set up at the AVGR is discussed in previous works (Heineck et al. 2002; Anderson et al. 2003). A brief description is given here. 3D PIV uses a system of lasers and cameras to image a horizontal slice of the ejecta curtain at specific times while the crater is growing. A laser plane is projected above and parallel to the target surface. At a specified time, the laser plane illuminates a horizontal ring of ejecta particles as they travel in the expanding ejecta curtain. Two CCD cameras, located above the target surface, image the illuminated ring of ejecta twice in rapid succession, allowing the ejecta particles to move slightly within the thickness of the laser plane.

A special software package (Lourenco and Krothapalli 1998) cross-correlates image pairs from each camera to track small groups of particles. For each camera this yields an array of two-dimensional displacement vectors which are then combined to give an array of three-dimensional displacements representing the motions of small groups of particles within the horizontal cross-section. The time delay between frames (ranging from 1 to 1000 μs, depending on the particle velocity) is incorporated into the displacements resulting in a final grid of three-dimensional velocity vectors, each representing a small group of ejecta particles within the laser plane. The software is accurate to within 2% for horizontal velocities and 4% for vertical velocities within the laser plane (Heineck et al. 2002). These three-dimensional velocities and positions completely determine the independent ballistic trajectories of the particles. The intersection of the ballistic trajectories with the pre-impact surface defines the ejection parameters, such as ejection speed and angle, in all directions around the impact point (Fig. 3). Using 3D PIV in conjunction with the oblique-angle capabilities of the AVGR provides the direct measurement of ejection position, speed, and angle in all azimuthal directions as the crater grows. The experiments used for this particular study specifically focus on the first half of the excavation stage of crater growth as the transient cavity radius expands to half the final crater radius.

Ejection angles for vertical impacts as a function of crater growth are plotted in Fig. 4 along with a comparison from Cintala et al. (1999). Contrary to results from non-dimensional scaling relationships (e.g., Housen et al. 1983), ejection angles are not constant for vertical impacts. Instead, ejection angles initially are high (55°) and then decrease (to 45°) up to approximately halfway through crater growth.

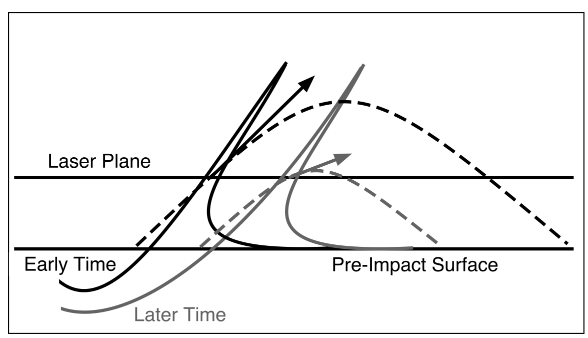

Fig. 3. 3D PIV measures the three-dimensional velocities of ejecta particles (arrows) within a horizontal laser plane located above and parallel to the target surface. At each time step, these measured velocity vectors completely define the ballistic trajectories of the ejecta particles (dashed lines). The intersection of the trajectories with the original target surface defines the ejection parameters such as ejection position, speed, and angle (from Anderson et al. 2003).

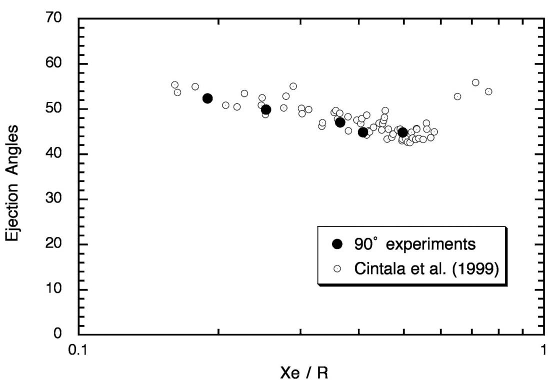

Fig. 4. Ejection angles measured using 3D PIV during vertical impacts are plotted versus ejection position, x_e, scaled by the final crater radius, R. The solid symbols are data from this study. The open symbols represent data from a similar experiment performed by Cintala et al. (1999) (from Anderson et al. 2003).

Through the last half of crater growth, experiments performed by Cintala et al. (1999) indicate that the ejection angles increase again. The data obtained for the present study do not extend to the latter half of crater growth; so, this trend is not yet observable.

Ejection angles also depend on azimuth around the impact point for oblique impacts (Figs. 5 through 8). The ejection angles with azimuth show a slight asymmetry at very early times for the 60° impacts and then flatten in azimuth as the crater grows (Fig. 5). The 45° impacts initially show lower ejection angles downrange than the average ejection angles for 90° impacts at roughly the same moment of crater growth (Fig. 6). The 30° impacts have distinctly asymmetric ejection angles with azimuth that persist well into the excavation stage of crater growth (Fig. 7). Finally, the 15° impacts also have much lower ejection angles downrange when compared to the average ejection angles for 90° impacts (Fig. 8).

In general, for all oblique impacts, the downrange ejection angles initially are between 4° and 15° lower than those of the vertical impacts, depending on the impact angle. The downrange ejection angles tend to increase as the crater grows and approach the average ejection angles observed for vertical impacts. Symmetry is never completely attained for the 30° and 15° impacts at the latest times shown here, approximately halfway through crater growth. Lateral ejection angles fall initially between the uprange and downrange values but increase to coincide with the uprange values at later times. Material ejected nearest the uprange direction for the oblique impacts tends to remain near the average ejection angle for the vertical impacts throughout crater growth. This initially may seem contradictory to previous studies that have measured observed ejecta curtain angles (as viewed from the side) that are significantly higher in the uprange direction. For example, Schultz and Anderson (1996) measured uprange curtain angles for a 45° impact initially to be near 70° and to decrease to near 50°, whereas

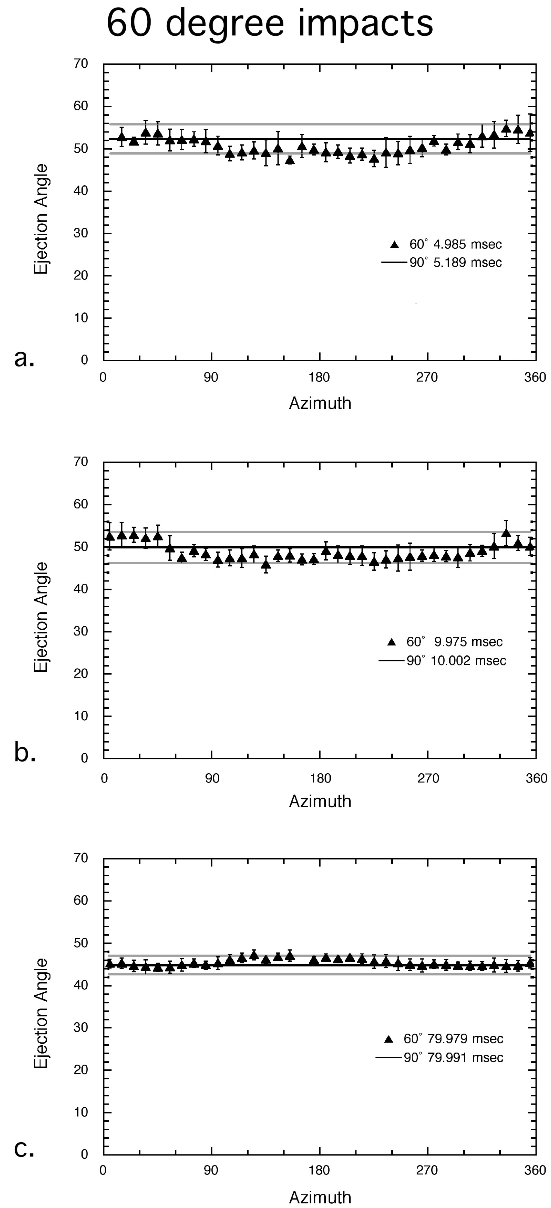

Fig. 5. Ejection angles measured using 3D PIV during 60° impacts plotted versus azimuth (solid symbols) for 3D PIV data obtained at roughly (a) 5 msec; (b) 10 msec; and (c) 80 msec after impact. The average ejection angle for vertical impacts measured at near the same time after impact is shown as a black line with one standard deviation in measured ejection angle represented by gray lines. The azimuth is defined as 0° directly uprange of the impact point, moving clockwise around the ejecta curtain to 180° directly downrange and back to 360° uprange. The lateral direction is perpendicular to the projectile trajectory (i.e., angles of 90° and 270° in azimuth). Average values of ejection angle are determined for each 10° azimuth bin. The error bars represent one standard deviation from the average ejection angle (some error bars may be smaller than the symbol). Slight differences between the lateral sides of the ejecta curtain are due to effects of lighting, as the laser plane originates from 270°. Note that the times shown in the figure do not refer to the ejection time. Rather, the time after impact is the sum of the ejection time and the time needed for the particles to move ballistically from the surface into the laser plane.

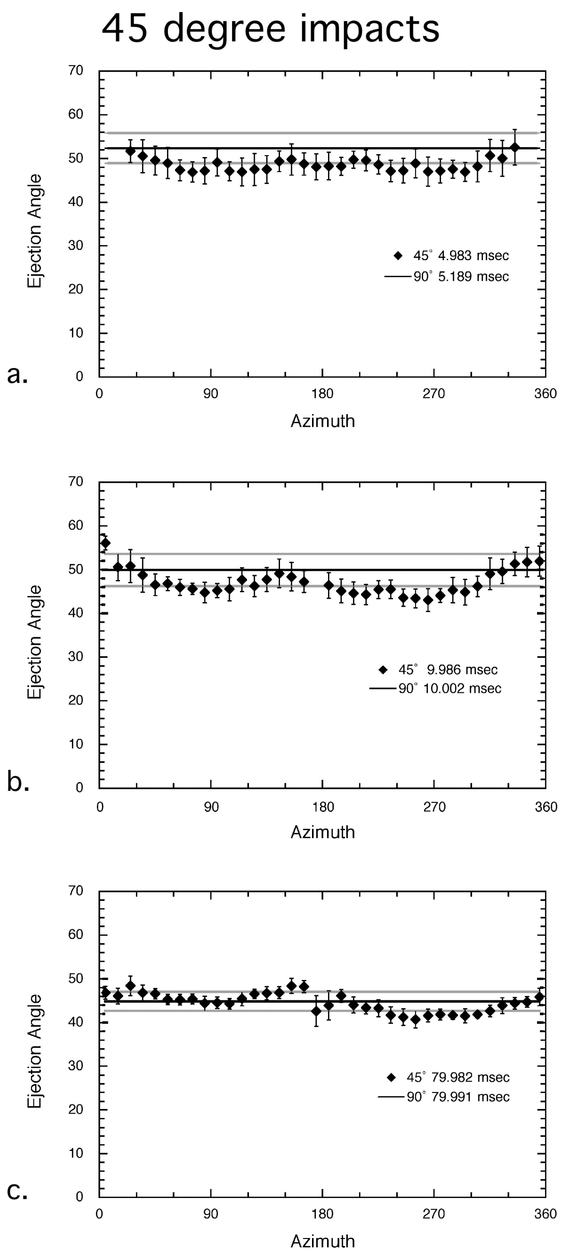

Fig. 6. Ejection angles from 45° impacts plotted versus azimuth in the same format as Fig. 5.

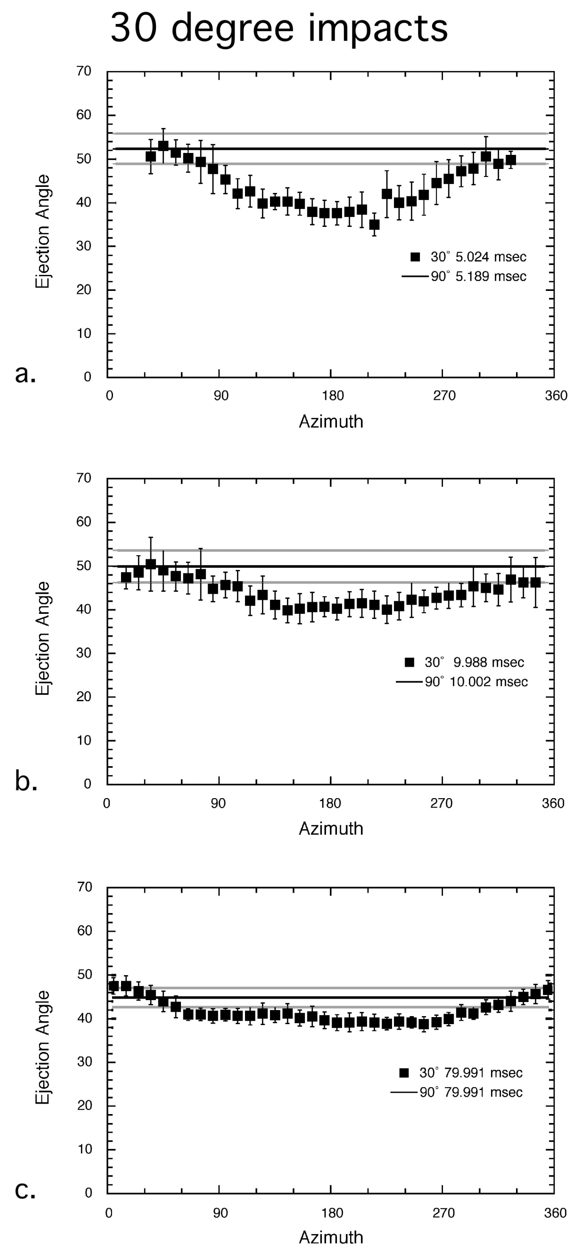

Fig. 7. Ejection angles from 30° impacts plotted versus azimuth in the same format as Fig. 5. Uprange data do not appear in (a) and (b) because the ejecta curtain has not yet closed in the uprange direction, and so there are no particles visible in the ejecta curtain at the laser plane yet.

this study shows uprange ejection angles for a 45° impact as dropping only from 52° to 46°. This difference reflects both perspective (viewing position) and fundamental differences between the ejecta curtain angle (measured as the angle of the inverted cone of ejecta moving outward) and individual ejecta particles' ejection angles (represented by the angle of the particles' ballistic trajectories as they pass through the target surface and derived using 3D PIV data). The ejecta curtain angle is an apparent angle made up by the positions of a number of different ejecta particles at different locations in flight along their ballistic trajectories frozen at one moment of crater growth. How the ejection angles change as the crater grows for the uprange segment will affect the ejecta curtain angle measured in a given instant in time. The evolving ejection angles derived using 3D PIV indicate an evolving flow-field beneath the target surface for both vertical and oblique impacts.

A point-source model can be used to represent the ejection process observed using 3D PIV during these experimental impacts. The measured ejection velocities, v_e,

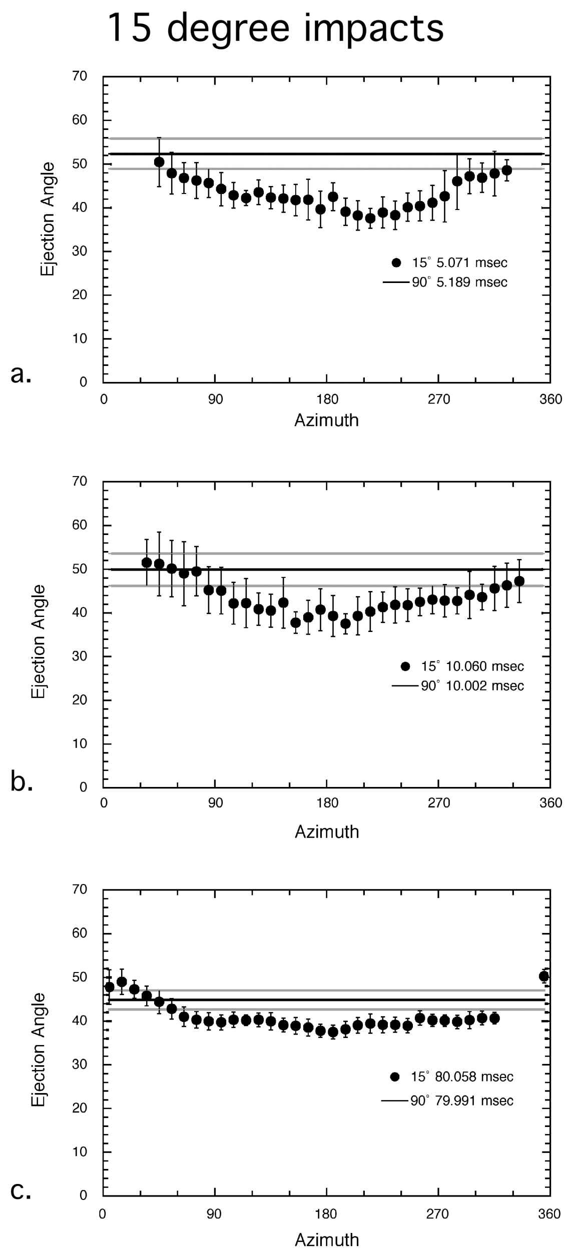

Fig. 8. Ejection angles from 15° impacts plotted versus azimuth in the same format as Fig. 5. Uprange data do not appear in (a) and (b) because the ejecta curtain has not yet closed in the uprange direction, and so there are no particles visible in the ejecta curtain at the laser plane yet. Data from 320° to 340° are missing in (c) because that section of the ejecta curtain was outside the camera's field of view.

as a function of ejection position, x_e, scale as predicted by dimensional analysis (Housen et al. 1983):

$$\frac{v_e}{\sqrt{gR}} \propto \left(\frac{x_e}{R}\right)^{-e_x} \tag{7}$$

where R is the final crater radius, and g is the gravitational acceleration. The exponent e_x is constant and represents the degree to which the impact is controlled by either momentum (e_x = 1.5) or energy (e_x = 3.0). The ejection velocity data obtained using 3D PIV for vertical impacts yield a value of e_x of 2.53 (Fig. 9), falling in between the theoretical limits for e_x and very close to the predicted value of 2.44 for impacts into Ottawa sand (Housen et al. 1983). This analysis implies that these experiments are following scaling relationships that are consistent with a point-source model.

The point-source model most often used to quantitatively represent the subsurface flow-field during an impact is the Z-Model. The next step, therefore, is to use the observed ejection angles in experimental impact craters to test the applicability of both the MZ-Model and the Z-Model in representing the subsurface flow-field for both vertical and oblique impacts.

THE MODIFIED Z-MODEL

3D PIV directly measures ejection angles for experimental impact craters as the crater is growing. These measured ejection angles can be used via inverse modeling to constrain the model parameters in Maxwell's original Z-Model (Equation 4) and the MZ-Model (Equation 6). Since numerous studies have shown that an impact is best modeled with a flow-field center located at some depth beneath the target surface, the MZ-Model was initially used in this study to determine the depth to the flow-field center and the best-fit value of Z. As shown below, the MZ-Model was able to predict the general evolution of the flow field for vertical impacts but was unable to predict the specific ejection angles for individual particles observed using 3D PIV, even for vertical impacts. This result emphasizes the detailed complexity of the crater excavation process.

The main limitation of the MZ-Model is its prediction of velocity vectors that point back toward the flow-field center as the crater first begins to grow (see Fig. 2). Using the MZ-Model (Equation 6), the evolution of predicted ejection angles can be observed for various values of Z in Fig. 10. When Z is held constant, tanΔ decreases with increasing distance from the flow-field center. At a certain distance away from the flow-field center, the subsurface streamlines defining the flow field emerge perpendicular to the target surface (θ_e = 90°). When Z is held constant at 3, this transition occurs at a distance of 1.7 d from the flow-field center (where d is the depth of the flow-field center). When Z is less than 3, vertical ejection angles are obtained nearer the flow-field center and vice versa for larger Z values. Thereafter, the ejection angles gradually decrease from vertical (90°) until tanΔ approaches zero, at which point the particles are approaching an infinite distance from the flow-field center; i.e., the flow-field center is effectively near the surface. When Z is held at 3, the MZ-Model never predicts ejection angles less than 45°. Ejection angles can be less than 45° provided that Z is lower than 3 but must be greater than

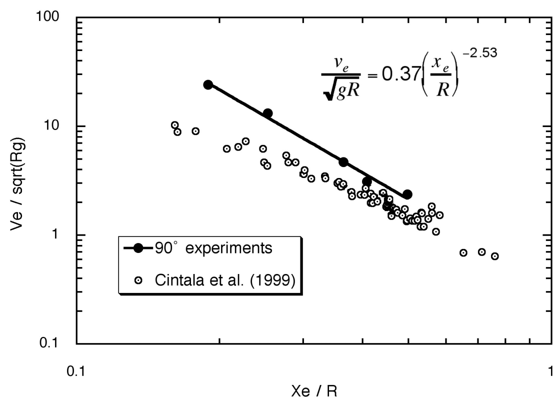

Fig. 9. Ejection velocities measured using 3D PIV during vertical impacts are plotted versus scaled ejection position (solid symbols). The open symbols represent data from a similar experiment performed by Cintala et al. (1999). Both data sets are within the bounds of energy- or momentum-scaling power relationships and, therefore, imply that a point-source approximation is valid for these experiments.

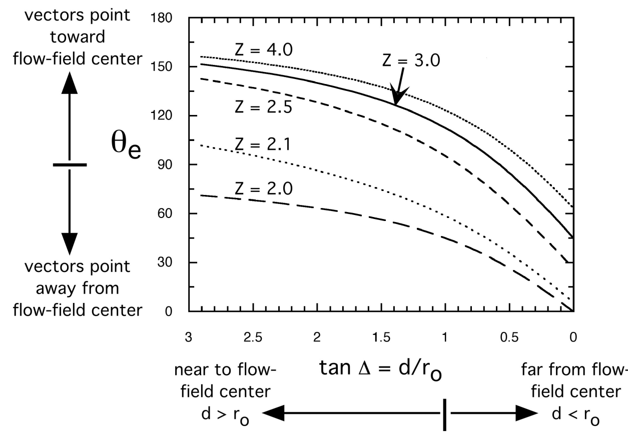

Fig. 10. Croft's Modified Z-Model (Equation 6) is limited by the relationship between tanΔ and Z. Here, ejection angles predicted by the MZ-Model are plotted versus tanΔ (the ratio of the depth to the flow-field center to the distance from the flow-field center in the x-direction; see Fig. 2). The predicted evolution of the ejection angles is shown for various values of Z, as material is ejected from near the flow-field center (large tanΔ) to far from the flow-field center (small tanΔ). Initially, for all Z >2, the MZ-Model predicts ejection angles that are higher than 90° corresponding to velocity vectors that point back toward the flow-field center. As the crater continues to grow, predicted ejection angles decrease, and eventually, all the different Z curves begin to predict velocity vectors that point away from the flow-field center. For Z = 3, this transition occurs when tanΔ = 0.6 (1.7 times the depth to the flow-field center) and, as the crater continues to grow, it is only possible to get ejection angles as low as 45°. For lower values of Z, ejection angles can continue to decrease below 45°. This continued and steady decrease in ejection angles throughout all of crater growth is not what is observed experimentally (see Fig. 4).

45° when Z is higher than 3. This result is strictly one involving the basic geometry of the subsurface streamlines in the MZ-Model and reflects streamlines that have been moved below the target surface by a constant amount representing the depth to the flow-field center (see Figs. 1 and 2). Consequently, the streamlines turn over upon themselves and predict velocity vectors that point back toward the flow-field center. When the depth to the flow-field center is increased, the problem worsens: velocity vectors pointing back toward the flow-field center are now predicted throughout a greater fraction of crater growth.

These observations lead to several general conclusions about using the MZ-Model to approximate the subsurface flow-field during vertical impacts. The MZ-Model allows for ejection angles to decrease as the crater grows, as is observed experimentally for vertical impacts (Fig. 4). In general, the MZ-Model is able to recreate the ejection speeds and angles observed for vertical impacts (Fig. 11) within reasonable estimates of Z, α, and d. In particular, the ejection angles are predicted much more realistically by the MZ-Model than by the original Z-Model. As the crater grows, the evolution of both ejection angle (Fig. 11a) and scaled ejection speed (Fig. 11b) are bounded by the MZ-Model. The MZ-Model gives a gross approximation to the instantaneous excavation flow-field at any given moment during crater growth for vertical impacts. The exact shape of the trend in ejection angle with scaled ejection position may (or may not) be fit exactly by one of the family of curves from the MZ-Model. Within the error (±4°) and range (currently x/R ~0.1 to 0.5) of the observed 3D PIV data, however, it is only possible to show that the MZ-Model matches the observed ejection angles better than the Z-Model. Hence, vertical impacts do require the inclusion of a term for the depth to the flow-field center.

The main limitation of the MZ-Model is its inability to predict ejection angles lower than a given value, depending on the chosen value for Z. Ejection angles below 45° are common in both vertical and oblique impacts (especially in the downrange direction; see Figs. 5–8). While the MZ-Model works reasonably well when used to predict average ejection angles for vertical impacts (Fig. 11a), the MZ-Model cannot predict the full range of ejection angles observed for individual ejecta particles using 3D PIV, even for vertical impacts. When given the observed ejection positions for particles during a vertical impact, the MZ-Model predicts a very large range of ejection angles that do not initially appear to match well with the observations (Fig. 12a). While the MZ-Model is an ineffective forward model to use with the 3D PIV data, the individual data do not invalidate the general conclusion that the MZ-Model provides a useful gross approximation to the subsurface flow-field at an instant in crater growth for vertical impacts. Given the sensitivity of the MZ-Model to the ejection position of the particles (see Fig. 10), slight differences in ejection positions that exist in the experimental data are enough to yield a large scatter in the predicted ejection angles from the MZ-Model. When the scatter plot in Fig. 12a is shown as a plot of number density (Fig. 12b), it can be seen that, overall, the vast majority of the observed ejection angles are predicted to within a few degrees by the MZ-Model. The average ejection angle observed for a

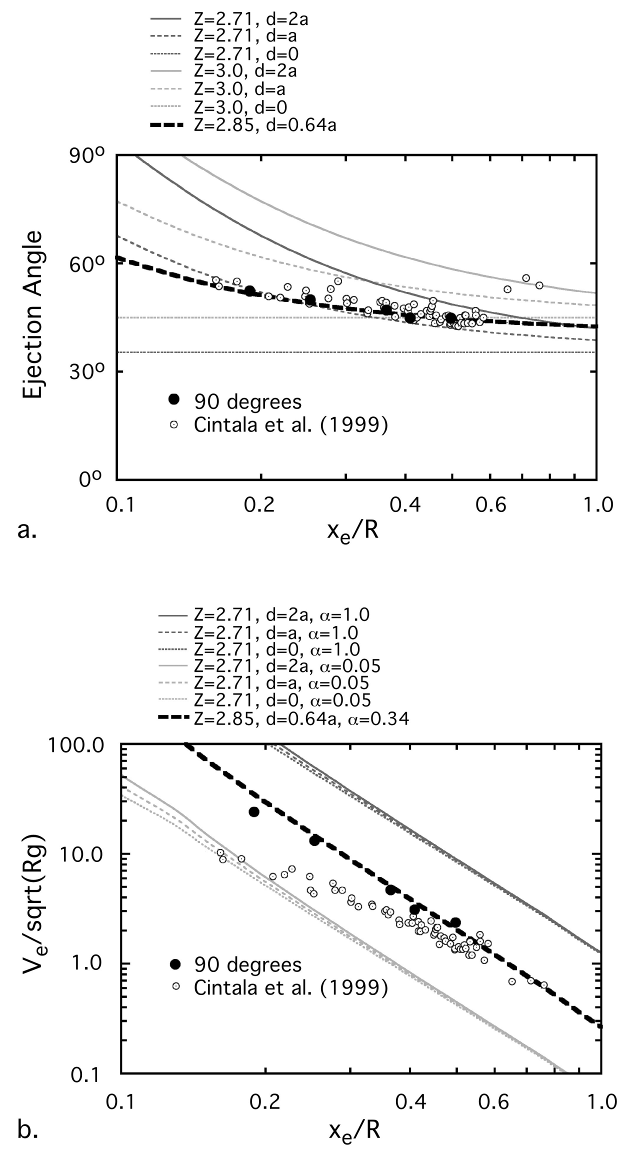

Fig. 11. Various predictions from the MZ-Model plotted with observed data for the ejection angle (a) and the scaled ejection speed (b) versus scaled ejection position for vertical impacts. In both cases, the 3D PIV data, as well as the data from Cintala et al. (1999), are bounded by the MZ-Model with reasonable assumptions for the model parameters, Z, α, and d: a) the MZ-Model is able to predict the general decrease in ejection angles as the crater grows for vertical impacts. Slight modifications to these standard assumptions give a better fit to the 3D PIV data as shown by the black dashed line for x_e/R from 0.1 to 0.5. In the MZ-Model, Z determines the asymptotic limit at $x/R = 1$, while the depth affects the amount of curvature near the flow-field center; b) the MZ-Model is also reasonable in predicting the power-law decrease in ejection speed for vertical impacts as the crater grows. In this case, the depth affects the slope only slightly, Z affects the slope dramatically, and α determines the intercept. For a small-scale impact calculation, α was found to range between 0.05 and 1.0 (Thomsen et al. 1979; Austin et al. 1980). These predictions bound the observed experimental data. The best value for α that fits the 3D PIV data is 0.34, shown by the dashed black line.

given moment of crater growth, therefore, can be predicted to within a few degrees even though the specific behavior of individual particles in the ejecta curtain from a vertical impact cannot be obtained from the MZ-Model. Such uncertainty is comparable to the standard deviation of the measured 3D PIV ejection angles.

As for oblique impacts, the MZ-Model is inadequate in predicting the observed ejection angles simply because it is unable to predict the wide range of ejection angles observed at any given moment during crater growth. Each curtain segment (e.g., uprange, downrange, and lateral) would require a separate MZ-Model, with independent values of Z, α, and d. In particular, the MZ-Model cannot predict the low ejection angles observed in the downrange portion of ejecta curtains from oblique impacts.

In summary, the MZ-Model is an improvement over Maxwell's original Z-Model as it allows for ejection angles to vary during crater growth for vertical impacts and reasonably matches experimental cratering observations (Fig. 11). The simple and straightforward addition of a depth term into Maxwell's Z-Model, however, cannot accurately predict ejection angles for oblique impacts. Perhaps the MZ-Model can be used to predict the average excavation parameters for explosion craters and vertical impacts by simply adding a linear depth term, but further refinement is needed to represent oblique impacts. This line of thought will be examined in more detail in a later section.

THE Z-MODEL AND OBLIQUE IMPACTS

Since the MZ-Model alone is not adequate to predict evolving ejection angles, can any information about the excavation of oblique impact craters be gleaned from Maxwell's original Z-Model? Initial studies using the Z-Model recognized the need for a depth term in impact cratering and estimated that depth by following the evolution of Z through time. Austin, Thomsen, and others (Thomsen et al. 1979; Austin et al. 1980, 1981) observed that the Z-Model could accurately represent the flow field at a given stage of crater growth, yielding a value for Z at that particular time. By stepping through time and fitting new values of Z and α to each time step, they observed the evolution of Z as the crater grew. This evolution of Z was interpreted as an influence of the changing depth to the flow-field center, since both Z and the depth alter the ejection angles. In general, higher Z values or a deeper flow-field center can produce the same ejection angles (Figs. 1 and 2). The remainder of this study follows previous studies (Thomsen et al. 1979; Austin et al. 1980, 1981) and works only with Maxwell's original Z-Model. Any evolution of Z with impact angle or ejection azimuth as the crater grows is interpreted to reflect the evolution of the depth to the flow-field center. This strategy examines whether or not the Z-Model can be modified differently to account for oblique impacts or if a new

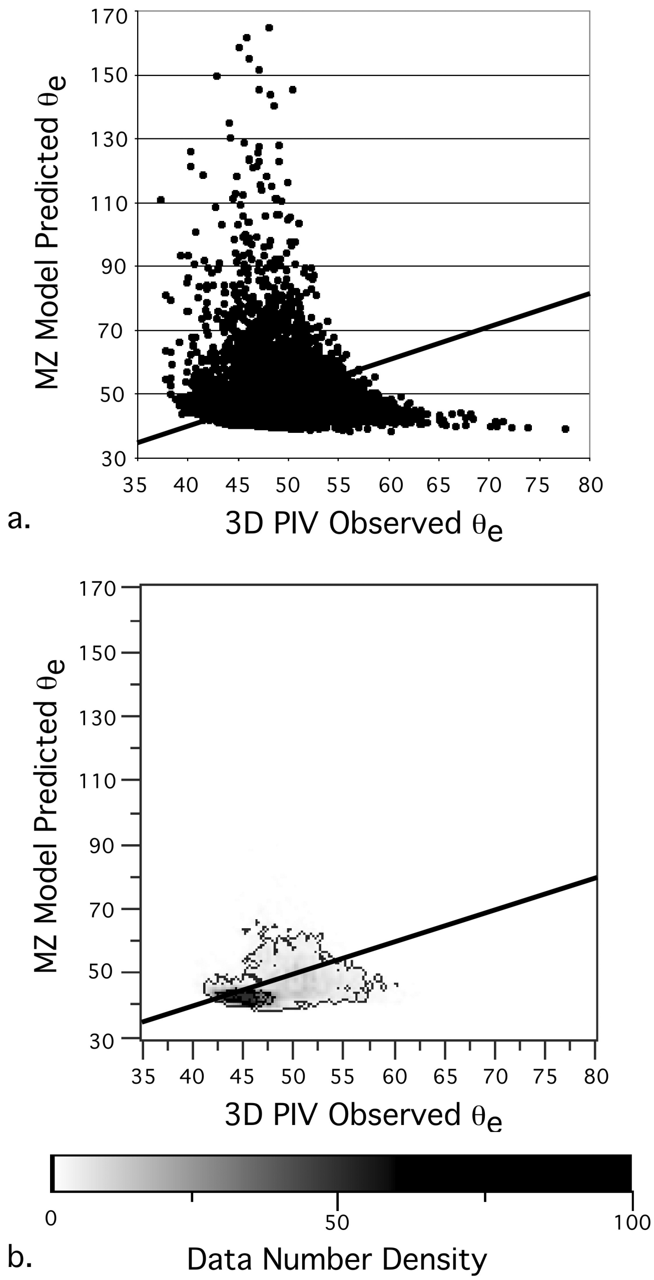

Fig. 12. a) Every individual ejection angle observed during vertical impacts using 3D PIV is plotted along the x-axis with corresponding ejection angles predicted by the MZ-Model on the y-axis. The solid black line represents a one-to-one correspondence. The MZ-Model predicts ejection angles above 90° when the ejection position is nearer the flow-field center; consequently, there is a greater spread in the predicted data than in the observed data. Such sensitivity of the MZ-Model to slight changes in ejection position make it an ineffective forward model to use for accurately predicting individual ejection angles; b) a shaded contour plot of the data density within (a), however, reveals general consistency between predicted and observed data. The first contour line represents regions with 5 or more data points and then the contours go upward every 50 data points. A one-to-one line is again shown for reference. This illustrates that the MZ-Model is reproducing the majority of the observed ejection angles to within a few degrees.

analytical model must be derived altogether to account for these new observations.

The method of assessing the depth of the flow-field center by observing the evolution of Z through time can be easily applied to the 3D PIV data. Since the present 3D PIV system builds the evolution of ejection angles as the crater grows by analyzing a series of nearly identical impacts (see Heineck et al. 2002; Anderson et al. 2003), each experiment will be used in the Z-Model inverse problem to satisfy Equation 4 to determine the best-fit value of Z for that stage of crater growth. Note that Equation 4 does not incorporate a depth to the flow-field center; consequently, this method assumes that the evolution of Z implies the migration of the flow-field center beneath the target surface. The problem becomes more difficult for oblique impacts because of the added dependence of ejection angle on azimuth (see Figs. 5–8). A first-order approximation for the effect of azimuth assumes that the value of Z for oblique impacts follows a linear dependence on the cosine of the azimuth, ϕ. In this case:

$$Z = Z_o + A\cos(\phi) \tag{8}$$

where Z_o is the average value of Z (and would represent the value of Z for a vertical impact where there is no azimuthal dependence), and A describes the amplitude of the azimuthal asymmetry expressed by the ejection angle. The azimuth ϕ = 0° for the uprange curtain segments and so $Z = Z_o + A$. Similarly, the downrange curtain segments (ϕ = 180°) yield $Z = Z_o - A$, and the lateral segments (ϕ = 90° or 270°) are simply $Z = Z_o$. An example of the ejection angles predicted by this azimuthally dependent Z value is shown in Fig. 13 and matches the observed data surprisingly well for such a simple modification. Even though the Z-Model may not accurately describe the asymmetric excavation of a crater formed by an oblique impact, results for the vertical and oblique impacts can be compared in order to contrast the predicted flow-fields.

Initial values of Z are high (Z = 3.3) for the vertical impacts (Fig. 14) but then decrease through the first 40% of crater growth, thereafter appearing to remain constant at about Z = 3 (at least to 50% of crater growth). This trend directly reflects the initially high ejection angles that decrease as the crater grows (Fig. 4). Maxwell's original Z-Model (Equation 4) determines the average ejection angle for each of the 90° data sets and its corresponding value of Z. Therefore, it is not surprising that values for Z also could be estimated using the ejection angles from Fig. 4. Since the present study only investigates the first half of crater growth, the continuing trend of the derived Z value cannot be assessed yet. Observations by Cintala et al. (1999) indicate that ejection angles increase through the last half of crater growth for similar experimental vertical impacts. Should the ejection angles indeed increase, then Z must also increase as the crater finishes its growth. The observed trend of Z for vertical impacts (Fig. 14) will be used as a benchmark for comparisons with data from oblique impacts.

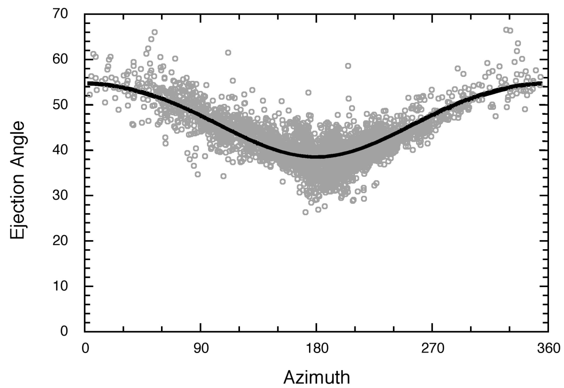

Fig. 13. During oblique impacts, such as this one at 30°, the ejection angle varies with azimuth. By approximating this variation as a linear function of Z with the cosine of the azimuth (Equation 8), it is possible to predict the variation in ejection angle for oblique impacts. The gray points are all of the observed ejection angles for this 30° impact and the black curve represents the predictions of the azimuthally dependent Maxwell's Z-Model.

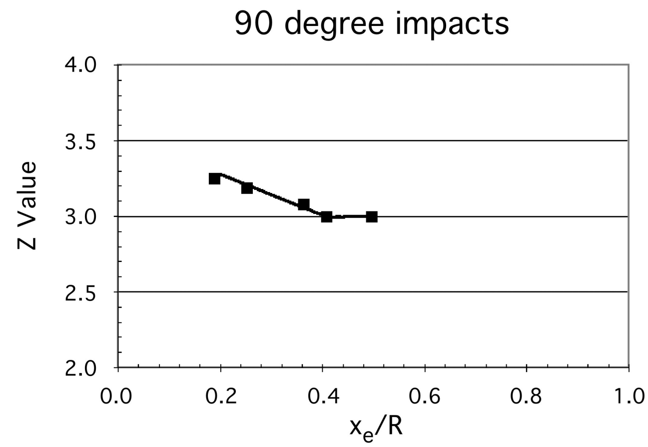

Fig. 14. The average Z value derived from observed ejection angles (Equation 2) plotted versus scaled ejection position for vertical impacts. In agreement with Fig. 4, Z is initially high, producing the observed high ejection angles; Z then decreases through the first half of crater growth until it appears to remain constant near 3. This evolution of Z is consistent with the migration of the center of the flow field upward from an initially deep position as the crater grows.

The same method is used for the oblique impacts with the addition of an azimuthal variation in Z (Equation 8). Values of Z_0 and A are determined for each experimental data set, and then Z for the uprange, downrange, and lateral curtain segments at that moment of crater growth is calculated following the form of Equation 8.

Impact angles studied here include 60°, 45°, 30°, and 15° above horizontal. All experiments involved low-velocity impacts (near 1 km/s) of 6.35 mm aluminum projectiles into medium-grained (0.5 mm average grain size) quartz sand. The evolution of Z for the 60° impacts follows the trend observed during vertical (90°) impacts very closely (Fig. 15a). Even when the curtain for the 60° impacts has been split into uprange, downrange, and lateral segments, Z values from all segments agree closely with those for the 90° impacts.

Values of Z for the uprange, downrange, and lateral curtain segments in the 45° impacts, however, depart from the 90° trend (Fig. 15b). The uprange values initially coincide with those for the 90° impacts, but the downrange values differ significantly. The trend of Z has a slope similar (although offset) to its vertical-impact counterpart but continues to decrease below 3. Z values for azimuths of 90° and 270° resemble those for a vertical impact.

The trend for 30° impacts differs considerably from that for 90° impacts (Fig. 15c). Again, the Z values for uprange ejecta roughly follow those from vertical impacts, while those in the lateral direction remain constant around a value of 3. Values of Z for the downrange direction, however, remain relatively constant at values near 2.8, falling below the 90° trend.

Lastly, the 15° values follow very interesting trends when compared to their 90° counterparts (Fig. 15d). The uprange values are consistently higher, whereas the lateral values coincide with the 90° trend. The downrange values are all near 2.8, well below the 90° trend but similar to the downrange values for the 30° impacts.

These values of Z represent the average Z needed to predict the average ejection angle observed for that particular segment of the curtain. The difference between ejection angles for 60° impacts as a function of azimuth and those for 90° impacts is minimal (Fig. 5); hence, the flow fields predicted by Maxwell's Z-Model are probably similar (Fig. 15a). Ejection angles begin to differ significantly from those for 90° impacts at impact angles somewhere between 45° and 60° (Figs. 6 and 15b) and become strongly azimuth-dependent at 30° (Figs. 7 and 15c). The 15° impacts are unique in that the projectile actually skips off the surface of the target at such low velocities (Schultz and Gault 1990). In this case, more than 70% of the energy and momentum is retained in the ricocheting projectile, resulting in flow fields from the 15° impacts that more closely resemble point sources than the 30° impacts. At the low velocities used here, the much smaller crater at 15° is centered closer to the impact point than is the case for the 30° impacts. This is in contrast to the trend exhibited as impact angles decrease from 60° to 30°, in which the center of the resulting crater becomes progressively offset farther downrange. This reflects a flow-field center that migrates downrange (from the impact point to the crater center) throughout crater growth. Therefore, trends of Z for the uprange, downrange, and lateral curtain segments for the 15° impacts are "cleaner" and approach the 90° impacts more closely than do the 30° impacts at this impact velocity (Fig. 15d).

The flow-field center is offset uprange from the geometric center of the final crater for all oblique impacts. The observed displacement between the impact point and the

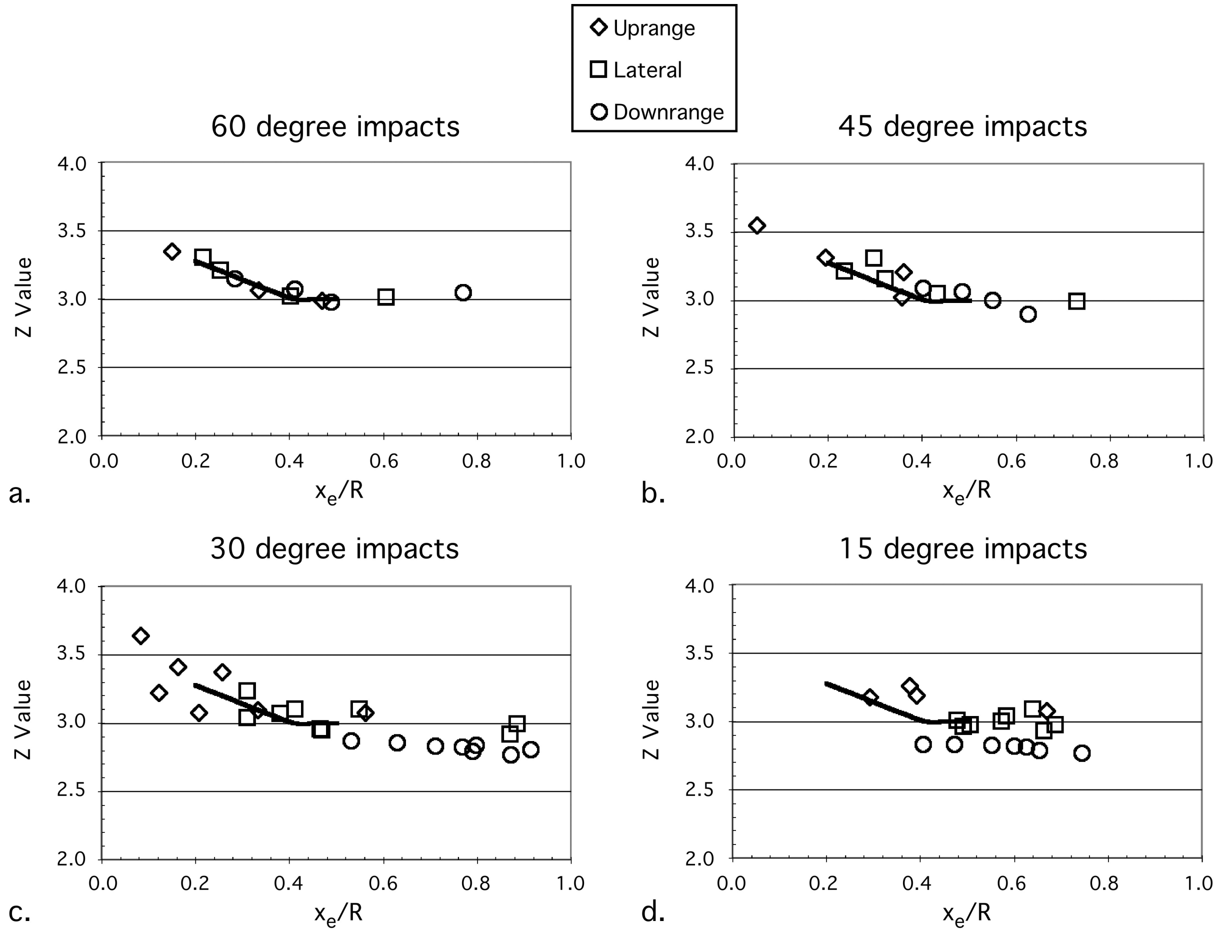

Fig. 15. The evolution of Z for oblique impacts versus scaled ejection position after inverting the Z-Model (Equation 2) while incorporating the cosine dependence for oblique impacts (Equation 8). Different values of Z have been determined for the uprange, downrange, and lateral curtain segments for: a) 60° impacts; b) 45° impacts; c) 30° impacts; and d) 15° impacts. The deviation of any of the trends from the trend for vertical impacts (black line) indicates that the flow fields predicted by the Z-Model for the oblique impacts differ significantly from those for the vertical impacts.

average crater center is as follows: 60° 2.27 ± 0.27 a; 45° 3.70 ± 0.36 a; 30° 4.19 ± 0.33 a; and 15° 3.17 ± 0.20 a, where *a* is the projectile diameter, and the stated errors are one standard deviation from the average value. Note that the average displacement for the 15° impacts is nearer that of the vertical impacts than even the 45° impacts at these low velocities.

The primary effect of the offset between the impact point and the crater center is the change in the relative distance from the flow-field center for each of the curtain segments (Anderson et al. 2002). Since the impact point is uprange of the crater center, particles ejected into the uprange portion of the ejecta curtain originate closer to the initial flow-field center. Downrange particles are ejected farther from the initial flow-field center (or impact point). The lateral particles, by definition, are not affected by this difference. Most likely, the flow-field center is initially near the impact point and migrates downrange toward the crater center. Consequently, Fig. 15 does not accurately depict the evolution of Z as the crater grows. A more correct model must incorporate the migrating flow-field center and will be the subject of a future study.

Two trends in the evolution of the flow-field center are observed in this study. First, Z values for both vertical and oblique impacts decrease through the first half of crater growth. This trend directly relates to the depth of the flow-field center within the target and implies that the flow-field center appears to migrate upward along the projectile's original trajectory for both vertical and oblique impacts. Second, the separation between the impact point and the final crater center for oblique impacts increases with decreasing impact angle and indicates that the flow-field center appears to migrate downrange at the same time as its depth decreases. Physically, these two trends reflect the superposition of two different flow fields that dominate crater growth at different times for both vertical and oblique impacts.

The two flow fields will be referred to as the momentum-driven flow-field and the excavation flow-field. The momentum-driven flow-field is characterized by an initially deep flow-field center created when the projectile penetrates into the target surface and downward flow initially dominates crater growth (the cavity grows downward to a maximum depth first). This evolution is exaggerated in highly porous targets (Schultz 2003). Later, the excavation flow-field develops in response to the point of maximum energy deposition and interactions with the free surface, and the crater grows laterally. In the case of vertical impacts, there is no horizontal component of momentum, and so the effects of the early momentum-driven flow-field are obscured by the later excavation flow-field. Oblique impacts, however, clearly expose the momentum-driven flow-field through azimuthal asymmetries in ejection angles and ejection velocities, especially in the downrange direction. The momentum-driven flow-field dominates the overall observed flow-field early in crater growth for both vertical and oblique impacts. As a result, ejection angles are high in all azimuths for the vertical impacts and are highly asymmetric in azimuth for oblique impacts. As the crater continues to grow, however, the momentum-driven flow-field decays more rapidly than the excavation flow-field. Consequently, the decreasing value of Z reflects the dominance of the excavation flow over the momentum-driven flow.

The effects of these two superimposed flow-fields are less distinct for low porosity targets and at very high velocities when the projectile decelerates rapidly and complete projectile failure occurs before significant penetration (e.g., Schultz and Gault 1985). In these cases, the momentum-driven flow-field is less pronounced because of the reduced capability of the projectile to create a deep penetration cavity. This accounts for the apparent contrast between this study and previous studies by Austin, Thomsen, and others (Thomsen et al. 1979; Austin et al. 1980, 1981). In their studies, projectiles impacted plasticene targets at high velocities. By requiring Z to be fixed at 2.11 directly below the impact point ($\Theta = 0°$), they found that the flow-field center migrated downward through crater growth. This conflicting result reflects differences in experimental conditions, namely low target porosity and high impact velocity, both of which act to minimize the downward-directed, momentum-driven flow during vertical impacts. The studies by Austin, Thomsen, and others followed the evolution of an excavation flow-field that was not as extensively affected by the momentum-driven flow-field as are the experiments described here.

In all the studies discussed here, it is agreed that the location of the flow-field center is not constant in time as the crater grows, for vertical impacts and especially for oblique impacts. This concept of an evolving flow-field center is consistent with previous observations of evolving centers of structural target failure both with depth into the target and parallel to the surface of the target (Schultz and Anderson 1996). The transition between momentum-driven flow and excavation flow is also reflected in the amount of ejecta directed downrange. Ejecta recovery experiments have shown that the ejecta mass per volume directed downrange exceeds expectations for gravity-controlled excavation from a point source (Schultz 1999; Schultz and Mustard Forthcoming) and can be explained by these two superimposed flow-fields. Direct measurements of asymmetries in peak pressures and momentum content within the far-field pressure wave (Dahl and Schultz 1999, 2001) also indicate an evolving source region at hypervelocities. Such asymmetries can be documented not only in the distribution of ejecta but also in structural asymmetries at planetary scales (Schultz 1992; Schultz and Anderson 1996; Dahl and Schultz 1999, 2001). These asymmetries include offset central peaks, breached peak rings, fracture patterns, and wall failure. Such asymmetries are not always evident in a statistical sense (Ekholm and Melosh 2001) due to mitigating effects of surface roughness, projectile failure (Venus), and crater size (circularization during collapse) as noted by Schultz (1992) and Schultz and Anderson (1996).

TOWARD A BETTER ANALYTICAL MODEL

3D PIV measurements of ejection angles for vertical and oblique impacts document an evolving subsurface flow-field as the crater grows. The superposition of two independently evolving flow-fields leads to a new understanding of the overall evolution of the subsurface flow-field for low-velocity impacts into particulate targets. For vertical impacts, the flow-field center predicted by Maxwell's Z-Model appears to migrate upward along its vertical trajectory directly beneath the impact point. For oblique impacts as high as 45°, the flow-field center begins to follow a different evolution and subsurface path than the flow-field center for vertical impacts. The flow-field center not only appears to move upward in the vertical direction (as with vertical impacts) but also migrate downrange along the trajectory. Maxwell's Z-Model is one specific example of a point-source model and the only analytical point-source approximation that has quantitative predictive features. Although the Z-Model accurately describes the subsurface flow-field geometry for explosions, it must be modified or rederived for detailing the evolution of impact craters.

Maxwell's Z-Model is not yet sufficiently accurate to describe observed excavation parameters (such as ejection angles) in detail, even for vertical impacts. The subsurface flow-field for both vertical and oblique impacts evolves in the four dimensions of space and time. Future analytical models of subsurface flow-fields must take this into account. The Z-Model was derived in only two spatial dimensions, and the flow-field center was assumed to be stationary. Croft's modification to the Z-Model simply added a constant depth term, displacing the flow field beneath the target surface. While such a strategy may accommodate the flow field for explosion cratering, the momentum of the impacting projectile is neglected (e.g., Dienes and Walsh 1970). Projectile momentum even affects the evolution of vertical impacts, causing the effective flow-field center to appear to migrate upward until the outward excavation flow dominates. In oblique impacts, the downrange component of the projectile's momentum affects the subsurface flow-field to an even greater degree and is more evident as the flow-field center appears to migrate both horizontally and vertically. In either case, whether vertical or oblique, the subsurface flow-field cannot be represented accurately by a single, stationary point-source. Furthermore, experimental data reveal that the flow field begins to change dramatically from that of vertical impacts at impact angles as high as 45°. Since this is the most common impact angle that forms craters on planetary surfaces, a better analytical model for the subsurface flow-field is needed to describe the excavation of the crater, final ejecta deposit, and transient crater shape and volume in the absence of a full-scale, three-dimensional numerical model.

The fact that the flow-field center evolves as the crater grows violates Maxwell's original assumption of incompressible flow along two-dimensional streamlines. Particles beneath the target surface will be responding to different flow-field centers as the crater grows. Consequently, they cannot be contained within one simple stream tube in two dimensions, even for vertical impacts. If Maxwell's original derivation were recast in three dimensions, however, it might be possible to retain the simplicity of the assumed streamlines. For example, Maxwell's observation that the radial velocity of the subsurface particles corresponds to the inverse power of the radial position (for explosions) may be correct as long as the radial position is always referenced to the instantaneous position of the flow-field center. Alternatively, a new relationship between the radial velocity and position of subsurface particles may soon emerge from three-dimensional numerical simulations of vertical and oblique impacts. Continued comparison between the results of numerical calculations, the predictions of point-source models (such as the Z-Model), and observations from experimental impacts will lead toward a better analytical model for impacts.

CONCLUSIONS

The following conclusions can be drawn from this study:

1. 3D PIV captures a continuously evolving flow-field through the first half of crater growth for both vertical and oblique impacts.
2. Maxwell's Z-Model can be used to interpret the evolving source regions in depth and position as functions of time for both vertical and oblique impacts.
3. Modifying Maxwell's Z-Model to incorporate an effective depth of a stationary point-source by simply moving the streamlines below the target surface by a constant amount (the MZ-Model) cannot accommodate the actual evolution of the flow field but remains useful in generally describing the excavation of vertical impacts.
4. Subsurface flow-fields developed during oblique impacts differ from their vertical counterparts at impact angles as high as 45°.
5. Observations of ejecta trajectories allow distinguishing between momentum-driven and excavation flow-fields in porous materials at low impact velocities. These results indicate that momentum-driven flow persists to as late as halfway through crater growth.
6. An analytical model fully tracing the evolving flow-field of an impact remains to be devised but may now be possible with the emerging detailed data from new experimental techniques.

In summary, oblique impacts differ significantly in flow-field geometry at impact angles as high as 45°. Since 45° is the most common impact angle on a planetary surface (Gilbert 1892; Shoemaker 1962), it is important to investigate the assumed flow-field geometry more closely and understand the effect of impact angle, especially at early times, on the subsurface flow, excavation, and subsequent deposition of material across planetary surfaces.

Acknowledgments–Many thanks to the NASA Ames Vertical Gun Range crew (D. Holt, R. Smythe, and D. Bowling) for their assistance and good humor during the experimental runs. We are also indebted to D. Forsyth and C. Cooper for many helpful conversations. The authors especially wish to thank the two reviewers of this manuscript, D. Orphal and M. Cintala, for their thorough reviews and extensive suggestions that greatly improved the clarity of this manuscript. This material is based on work supported by a National Science Foundation Graduate Research Fellowship, a NASA-Rhode Island Space Grant Graduate Student Fellowship and NASA Grant No. NAG5–11538.

Editorial Handling—Dr. E. Pierazzo and Dr. R. Herrick

REFERENCES

Anderson J. L. B., Schultz P. H., and Heineck J. T. 2002. Evolving flow-field centers in oblique impacts (abstract #1762). 33rd Lunar and Planetary Science Conference. CD-ROM.

Anderson J. L. B., Schultz P. H., and Heineck J. T. 2003. Asymmetry of ejecta flow during oblique impacts using three-dimensional particle image velocimetry. *Journal of Geophysical Research* 108, doi: 10.1029/2003JE002075.

Artemieva N. A. and Pierazzo E. 2003. Oblique impact and its ejecta—Numerical modeling (abstract #8022). Workshop on Impact Cratering: Bridging the Gap Between Modeling and Observations.

Austin M. G., Thomsen J. T., Ruhl S. F., Orphal D. L., and Schultz P. H. 1980. Calculational investigation of impact cratering dynamics: Material motions during the crater growth period. Proceedings, 11th Lunar and Planetary Science Conference. pp. 2325–2345.

Austin M. G., Thomsen J. M., Ruhl S. F., Orphal D. L., Borden W. F., Larson S. A., and Schultz P. H. 1981. Z-model analysis of impact cratering: An overview. In *Multi-ring basins,* edited by Schultz P. H. and Merrill R. B. New York: Pergamon Press. pp. 197–205.
Baldwin R. B. 1963. *The measure of the Moon.* Chicago: University of Chicago Press. 488 p.
Chabai A. J. 1965. On scaling dimensions of craters produced by buried explosives. *Journal of Geophysical Research* 70:5075–5098.
Chabai A. J. 1977. Influence of gravitational fields and atmospheric pressures on scaling of explosion craters. In *Impact and explosion cratering,* edited by Roddy D. J., Pepin R. O., and Merrill R. B. New York: Pergamon Press. pp. 1191–1214.
Cintala M. J., Berthoud L., and Hörz F. 1999. Ejection-velocity distributions from impacts into coarse-grained sand. *Meteoritics & Planetary Science* 34:605–623.
Collins G. S., Melosh H. J., Morgan J. V., and Warner M. R. 2002. Hydrocode simulations of Chicxulub crater collapse and peak-ring formation. *Icarus* 157:24–33.
Cooper H. F. 1977. A summary of explosion cratering phenomena relevant to meteor impact events. In *Impact and explosion cratering,* edited by Roddy D. J., Pepin R. O., and Merrill R. B. New York: Pergamon Press pp. 11–44.
Croft S. K. 1980. Cratering flow fields: Implications for the excavation and transient expansion stages of crater formation. Proceedings, 11th Lunar and Planetary Science Conference. pp. 2347–2378.
Dahl J. M. and Schultz P. H. 1999. In-target stress wave momentum content in oblique impacts (abstract #1854). 30th Lunar and Planetary Science Conference. CD-ROM.
Dahl J. M. and Schultz P. H. 2001. Measurement of stress wave asymmetries in hypervelocity projectile impact experiments. *International Journal of Impact Engineering* 26:145–155.
Dienes J. K. and Walsh J. M. 1970. Theory of impact: Some general principles and the method of Eulerian codes. In *High-velocity impact phenomena,* edited by Kinslow R. New York: Academic Press. pp. 45–104.
Ekholm A. G. and Melosh H. J. 2001. Crater features diagnostic of oblique impacts: The size and position of the central peak. *Geophysical Research Letters* 28:623–626.
Gault D. E. and Wedekind J. A. 1977. Experimental hypervelocity impact into quartz sand—II, Effects of gravitational acceleration. In *Impact and explosion cratering,* edited by Roddy D. J., Pepin R. O., and Merrill R. B. New York: Pergamon Press pp. 1231–1244.
Gault D. E. and Wedekind J. A. 1978. Experimental studies of oblique impact. Proceedings, 9th Lunar and Planetary Science Conference. pp. 3843–3875.
Gilbert G. K. 1892. The Moon's face. *Bulletin of the Philosophical Society of Washington* 12:241–292.
Grieve R. A. F. and Cintala M. J. 1981. A method for estimating the initial impact conditions of terrestrial cratering events, exemplified by its application to Brent crater, Ontario. Proceedings, 12th Lunar and Planetary Science Conference. pp. 1607–1621.
Heineck J. T., Schultz P. H., and Anderson J. L. B. 2002. Application of three-component PIV to the measurement of hypervelocity impact ejecta. *Journal of Visualization* 5: 233–241.
Holsapple K. A. 1980. The equivalent depth of burst for impact cratering. Proceedings, 11th Lunar and Planetary Science Conference. pp. 2379–2401.
Holsapple K. A. and Schmidt R. M. 1982. On the scaling of crater dimensions: Impact processes. *Journal of Geophysical Research* 87:1849–1870.
Holsapple K. A. and Schmidt R. M. 1987. Point source solutions and coupling parameters in cratering mechanics. *Journal of Geophysical Research* 92:6350–6376.
Holsapple K. A. 1993. The scaling of impact processes in planetary sciences. *Annual Review of Earth and Planetary Sciences* 21: 333–373.
Housen K. R., Schmidt R. M., and Holsapple K. A. 1983. Crater ejecta scaling laws: Fundamental forms based on dimensional analysis. *Journal of Geophysical Research* 88:2485–2499.
Kreyenhagen K. N. and Schuster S. H. 1977. Review and comparison of hypervelocity impact and explosion cratering calculations. In *Impact and explosion cratering,* edited by Roddy D. J., Pepin R. O., and Merrill R. B. New York: Pergamon Press. pp. 983–1002.
Lourenco L. M. and Krothapalli A. 1998. Mesh-free, second-order accurate algorithm for PIV processing. Paper presented at the International Conference on Optical Technology and Image Processing in Fluid, Thermal, and Combustion Flow. Society of Photo-Otpical Instrumentation Engineers. Yokohama, Japan.
Maxwell D. E. 1973. *Cratering flow and crater prediction methods.* San Leandro: Physics International Company. 50 p.
Maxwell D. E. 1977. Simple Z model of cratering, ejection, and the overturned flap. In *Impact and explosion cratering,* edited by Roddy D. J., Pepin R. O., and Merrill R. B. New York: Pergamon Press. pp. 1003–1008.
Oberbeck V. R. 1971. Laboratory simulation of impact cratering with high explosives. *Journal of Geophysical Research* 76:5732–5749.
Oberbeck V. R. 1977. Application of high explosion cratering data to planetary problems. In *Impact and explosion cratering,* edited by Roddy D. J., Pepin R. O., and Merrill R. B. New York: Pergamon Press. pp. 45–65.
Orphal D. L. 1977. Calculations of explosion cratering II: Cratering mechanics and phenomenology. In *Impact and explosion cratering,* edited by Roddy D. J., Pepin R. O., and Merrill R. B. New York: Pregamon Press. pp. 907–917.
Piekutowski A. J. 1977. Cratering mechanisms observed in laboratory-scale high-explosive experiments. In *Impact and explosion cratering,* edited by Roddy D. J., Pepin R. O., and Merrill R. B. New York: Pergamon Press. pp. 67–102.
Piekutowski A. J. 1980. Formation of bowl-shaped craters. Proceedings, 11th Lunar and Planetary Science Conference. pp. 2129–2144.
Pierazzo E. and Melosh H. J. 1999. Hydrocode modeling of Chicxulub as an oblique impact event. *Earth and Planetary Science Letters* 165:163–176.
Pierazzo E. and Melosh H. J. 2000a. Hydrocode modeling of oblique impacts: The fate of the projectile. *Meteoritics & Planetary Science* 35:117–130.
Pierazzo E. and Melosh H. J. 2000b. Understanding oblique impacts from experiments, observations, and modeling. *Annual Review of Earth and Planetary Sciences* 28:141–167.
Roddy D. J. 1968. The Flynn Creek crater, Tennessee. In *Shock metamorphism of natural materials,* edited by French B. M. and Short N. M. Baltimore: Mono Book Corporation. pp. 291–322.
Roddy D. J. 1976. High-explosive cratering analogs for bowl-shaped, central uplift and multiring impact structures. Proceedings, 7th Lunar and Planetary Science Conference. pp. 3027–2056.
Schmidt R. M. and Holsapple K. A. 1980. Theory and experiments on centrifuge cratering. *Journal of Geophysical Research* 85: 235–252.
Schmidt R. M. and Housen K. R. 1987. Some recent advances in the scaling of impact and explosion cratering. *International Journal of Impact Engineering* 5:543–560.
Schultz P. H. and Gault D. E. 1985. The effect of projectile shape on cratering efficiency and crater profile in granular targets. 16th Lunar and Planetary Science Conference. pp. 742–743.

Schultz P. H. 1988. Cratering on Mercury: A relook. In *Mercury,* edited by Vilas F., Chapman C. R., and Matthews M. S. Tucson: University of Arizona Press. pp. 274–335.

Schultz P. H. and Gault D. E. 1990. Prolonged global catastrophes from oblique impacts. In *Global catastrophes in Earth history; An interdisciplinary conference on impacts, volcanism, and mass mortality,* edited by Sharpton V. L. and Ward P. D. Boulder: Geological Society of America. pp. 239–261.

Schultz P. H. 1992. Atmospheric effects on ejecta emplacement and crater formation on Venus from Magellan. *Journal of Geophysical Research* 97:16183–16248.

Schultz P. H. and Anderson R. R. 1996. Asymmetry of the Manson impact structure: Evidence for impact angle and direction. Geological Society of America Special Paper 302. pp. 397–417.

Schultz P. H. 1999. Ejecta distribution from oblique impacts into particulate targets (abstract #1919). 30th Lunar and Planetary Science Conference. CD-ROM.

Schultz P. H. 2003. Transient crater growth in low density targets (abstract #2067). 34th Lunar and Planetary Science Conference. CD-ROM.

Schultz P. H. and Mustard J. F. Forthcoming. Impact melts and glasses on Mars. *Journal of Geophysical Research.*

Shoemaker E. M. 1962. Interpretation of lunar craters. In *Physics and astronomy of the Moon,* edited by Kopal Z. New York: Academic Press. pp. 283–359.

Stöffler D., Gault D. E., Wedekind J. A., and Polkowski G. 1975. Experimental hypervelocity impact into quartz sand: Distribution and shock metamorphism of ejecta. *Journal of Geophysical Research* 80:4062–4077.

Thomsen J. T., Austin M. G., Ruhl S. F., Schultz P. H., and Orphal D. L. 1979. Calculational investigation of impact cratering dynamics: Early time material motions. Proceedings, 10th Lunar and Planetary Science Conference. pp. 2741–2756.

Turtle E. P., Pierazzo E., and O'Brien D. P. 2003. Numerical modeling of impact heating and cooling of the Vredefort impact structure. *Meteoritics & Planetary Science* 38:293–303.